Charge-transfer complexes of sulfur-rich acceptors derived from birhodanines†

Shuxiang Fan,[a] Yasuhiro Kiyota,[a] Kodai Iijima,[a] Suho Ryo,[a] Tadashi Kawamoto,[a] Yann Le Gal,[b] Dominique Lorcy,[b] and Takehiko Mori*[a]

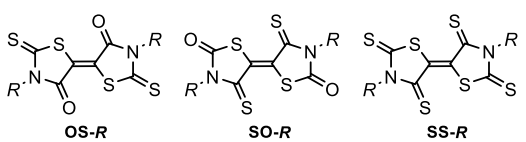
Sulfur-rich acceptors, birhodanines, 3,3'-dialkyl-5,5'-bithiazolidinylidene-2,2'-dione-4,4'-dithiones (**OS-*R***, *R* = Et and Pr) and 3,3'-dialkyl-5,5'-bithiazolidinylidene-4,4'-dione-2,2'-dithiones (**SO-*R***, *R* = Et), as well as the sulfur analogues, 3,3'-dialkyl-5,5'-bithiazolidinylidene-2,4,2',4'-tetrathiones (**SS-*R***, *R* = Et, Pr), form 1:1 composition charge-transfer complexes with donors such as pyrene, perylene, and coronene. These complexes have mixed stacks, and the **SS-*R*** complexes show n-channel transistor properties due to the intercolumnar S···S contacts between the acceptors. By contrast, the **OS-*R*** and **SO-*R*** complexes exhibit basically hole-dominant ambipolar properties due to the absence of S···S contacts. Accordingly, the charge transport is governed mostly by the direct interchain interactions instead of the transport along the columns.

Introduction

Recently, we have reported n-channel transistor materials with excellent air stability: birhodanines, 3,3'-dialkyl-5,5'-bithia zolidinylidene-2,2'-dione-4,4'-dithiones (Scheme 1, hereafter abbreviated as **OS-*R***), as well as the isomer, 3,3'-dialkyl-5,5'-bithiazolidinylidene-4,4'-dione-2,2'-dithiones (**SO-*R***) and their sulfur analogues, 3,3'-dialkyl-5,5'-bithiazolidinylidene-2,4,2',4'-tetrathiones (**SS-*R***).[1-3] **SS-*R*** is obtained in the course of developing single-component molecular conductors,[4,5] and is a sufficiently strong electron acceptor to achieve air-stable n-channel transistors. **OS-*R*** and **SO-*R*** are a little weaker acceptors and the device air stability is slightly reduced. Despite their strong acceptor ability, these acceptors have been very little studied as precursor of charge transfer complexes. Only a ferrocene complex of **SS-Et** together with the ferrocene and tetramethyltetrathiafulvalene complexes of the dicyanomethylene derivative have been reported;[5] these combinations exhibit mixed-stack structures.

However, there is recently an increasing interest in charge-transfer complexes of organic semiconductors.[6] This is partly prompted by increasing attention to the carrier doping;[7] formation of a structurally well-defined donor-acceptor (DA) cocrystal is unmistakable evidence of the charge-transfer interaction. Transistor properties of such charge-transfer complexes have been investigated,[8] which are interesting in analogy with the recently developing high-performance DA polymers.[9]

Since DA complexes contain both D and A units, it is likely that DA cocrystals show ambipolar transistor properties. In mixed-stack complexes, both electron and hole transports are subjected to the same hopping process between the D highest occupied molecular orbital (HOMO) and the A lowest unoccupied molecular orbital (LUMO). When such a process is characterized by a transfer integral t and energy difference $E_L - E_H$, the effective electron and hole transfers are represented by $t_e^{eff} \sim t_h^{eff} \sim t^2/(E_L - E_H)$, and should be the same.[10] Nonetheless, many DA cocrystals show only n-channel transport, particularly in tetracyanoquinodimethane (TCNQ) complexes.[8,11] This is because the D HOMO and the A LUMO are approximately orthogonal ($t \sim 0$) due to the horizontal node of the D HOMO.[12-15] The electron transport is usually mediated by the hybridization of the D next HOMO (HOMO−1), which has the same stripe symmetry as the A LUMO. There are no such "bridge" orbitals to mediate hole transport, and electron-only transport has been universally observed.[13]



Scheme 1. Molecular structures, where *R* = ethyl (Et), and *n*-propyl (Pr).

Accepted manuscript

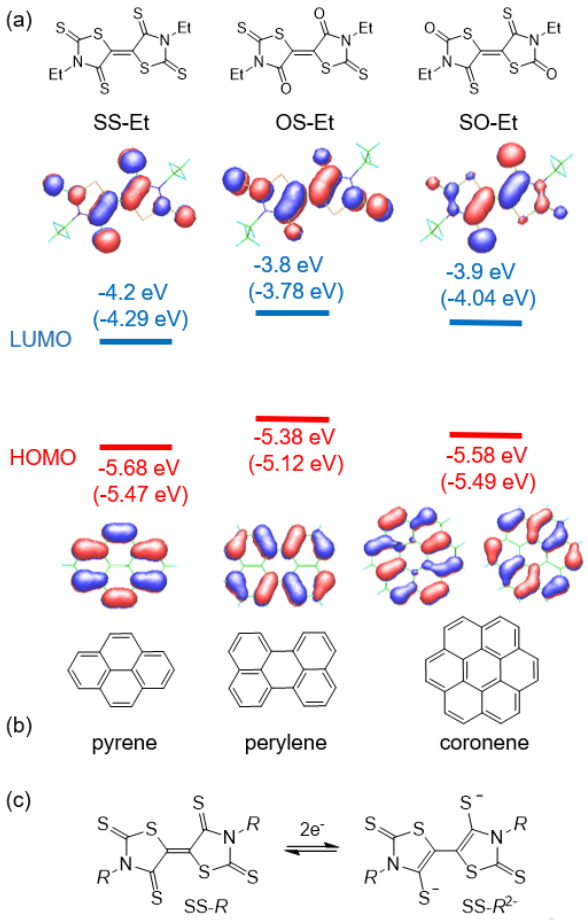


Figure 1. (a) Molecular orbitals of **SS-Et**, **OS-Et**, and **SO-Et** as well as (b) pyrene, perylene, and coronene. The energy levels are determined by cyclic voltammetry.[2,14,15] The values in the parentheses are from the molecular orbital calculations. (c) Anionic form of **SS-*R***.

The present paper reports crystal structures and transistor properties of pyrene, perylene, and coronene (Fig. 1) complexes of **SS-*R*, OS-*R*** and **SO-*R*** acceptors (*R* = Et and Pr). These cocrystals have mixed-stack columns, though the details depend on the alkyl chains and donors. **SS-*R*** complexes exhibit electron-transporting transistor properties, whereas **OS-*R*** and **SO-*R*** complexes show basically ambipolar transistor properties. The transistor properties are discussed by investigating the intermolecular interactions.

Experimental section and calculation method

The acceptor molecules were prepared according to the reported methods.[2,5] The acceptors and the donors were independently dissolved in warm toluene, and the solvent of the mixed solution was slowly evaporated. After about three weeks, black needle-like crystals were harvested. Acceptors with *R* = methyl, ethyl, *n*-propyl, and *n*-butyl were combined with various donors, among which crystals with sufficient quality were obtained for combinations listed in Tables 1 and 2.

Transistors were fabricated onto n-doped Si substrates with a thermally grown SiO_2 dielectric layer (300 nm, C = 11.5 nF cm^{-2}). The passivation layer polystyrene (PS, ε = 2.5) was deposited by spin coating (3000 rpm and 30 sec) a solution of PS (20 mg) in toluene (1 mL) on the substrates with a thickness of 100 nm,[16] where the calculated overall capacitance was 7.6 nF cm^{-2}.[17] Needle-like black crystals were put on the PS layer using ethanol.[18] Carbon paste (DOTITE, XC-12) was deposited on two ends of the single crystal to make the source and drain electrodes, and the crystal long axis was oriented in the channel direction. The single-crystal X-ray diffraction indicates that the crystal long axis is parallel to the molecular stacking axis. The transistor properties were measured under the vacuum of 10^{-3} Pa by using a Keithley 4200 semiconductor parameter analyzer.

Molecular orbital calculations in the B3LYP* level with TZP basis set were performed using the Amsterdam Density Functional (ADF) program.[19] Direct AA/DD transfers were evaluated from the splitting of A LUMO/D HOMO in the AA/DD dimers. Direct transfers were also estimated from the frozen orbital approximation.[20,21] In the mixed stacks, t_e^{eff}/t_h^{eff} was evaluated from the LUMO/HOMO splitting of an ADA/DAD triad.[10,13] t_e^{eff} and t_h^{eff} were also obtained from the partition method according to the following equation.[12,13]

$$t^{eff} = \sum_i \frac{t_{0i} t_{i0}}{E_0 - E_i} \quad (1)$$

Results and discussion

Energy levels and molecular orbitals

Energy levels and molecular orbitals are shown in Fig. 1. **SS-*R*** is a strong electron acceptor with the LUMO level at −4.2 eV,[2] which is sufficient to achieve air-stable n-channel transistors. This is because we can suppose an S^- form for the anion as depicted in Fig. 1(c), where the LUMO is delocalized to the C=S parts. **OS-*R*** and **SO-*R*** are a little weaker acceptors with the LUMO level at −3.8 eV ~ −3.9 eV,[2] and the transistor air stability is slightly reduced. Perylene and coronene are moderate electron donors, whereas pyrene is a weak electron donor.[14,15] The resulting HOMO-LUMO gaps of the complexes are located in the range of 1.2-1.9 eV.

Crystal structures

X-ray single-crystal structure analyses were carried out for five **SS-*R*** complexes (*R* = Et and Pr) listed in Table 1 as well as three **OS-*R*** (*R* = Et and Pr) and three **SO-Et** complexes listed in Table 2. Perylene makes crystals with all these five acceptors.

These complexes have mixed stacks along the *b* axis (Figs. 2-4). These crystals are, however, not strictly isostructural; the lattice angles are considerably different in the **OS-*R*** complexes (Table 2). The DA interplanar spacings, listed in Tables 2 and

Accepted manuscript

Table 1. Crystallographic data of **SS-*R*** complexes.

	(pyrene) (**SS-Et**)	(perylene) (**SS-Et**)	(coronene) (**SS-Et**)	(pyrene) (**SS-Pr**)	(perylene) (**SS-Pr**)
Formula	$C_{26}H_{20}N_2S_6$	$C_{30}H_{22}N_2S_6$	$C_{34}H_{22}N_2S_6$	$C_{28}H_{24}N_2S_6$	$C_{32}H_{26}N_2S_6$
Formula weight	552.82	602.88	650.92	580.87	630.93
Crystal System	triclinic	triclinic	triclinic	monoclinic	monoclinic
Space Group	$P\bar{1}$	$P\bar{1}$	$P\bar{1}$	$P2_1/n$	$P2_1/c$
Shape	block	block	block	block	plate
a (Å)	7.457(5)	7.541(6)	7.271(3)	7.564(3)	7.659(8)
b (Å)	7.942(8)	8.263(6)	9.426(9)	7.574(6)	8.117(6)
c (Å)	11.259(7)	11.632(7)	11.546(6)	22.84(1)	23.27(3)
α (deg.)	71.93(6)	70.08(5)	67.88(5)	90	90
β (deg.)	74.01(5)	75.07(6)	74.83(4)	96.90(3)	96.74(8)
γ (deg.)	89.57(7)	89.43(7)	79.16(5)	90	90
V (Å^3)	607.2(8)	656.0(8)	703.9(9)	1299(1)	1437(3)
Z-value	1	1	1	2	2
T (K)	298	298	298	298	298
D_{calc} (g cm^{-3})	1.512	1.526	1.535	1.485	1.459
Total reflns.	4199	4554	4808	4500	4828
Unique reflns. (R_{int})	3545 (0.0592)	3836 (0.0985)	4116 (0.0463)	3792 (0.0219)	4201 (0.0255)
R_1 [$F^2 > 2\sigma(F^2)$]	0.0454	0.0530	0.0538	0.0401	0.0556
wR_2 [All reflections]	0.1323	0.1543	0.1582	0.1144	0.1656
GOF	1.020	0.999	1.000	1.050	0.927
DA spacing (Å)	3.47	3.50	3.49	3.51	3.52
S···S contacts (Å)	4.06, 4.08	3.59	3.56	3.90, 4.08	3.96

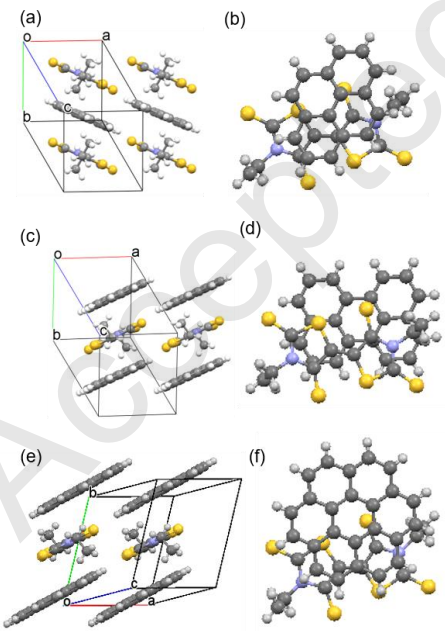


Figure 2. (a) Crystal structure of (pyrene)(**SS-Et**) viewed along the acceptor long axis, and (b) viewed perpendicular to the molecular plane. (c) Crystal structure of (perylene)(**SS-Et**) viewed along the acceptor long axis, and (b) viewed perpendicular to the molecular plane. (d) Crystal structure of (coronene)(**SS-Et**) viewed along the acceptor long axis, and (e) viewed perpendicular to the molecular plane.

3, are around 3.50 Å in the **SS-*R*** and **SO-*R*** complexes, but about 3.45 Å in the **OS-*R*** complexes. The difference indicates that the inner C=O decreases the DA spacing slightly. At the same time, **SS-Pr** complexes have larger DA spacings than **SS-Et** complexes (Table 1); a long alkyl chain increases the interplanar spacings. These tendencies are also observed in neutral **SS-*R*** and **OS-*R***.[2,3]

The stack is not the ordinary face-to-face stack but tilted along the molecular short axis (Fig. 2(a)). The neutral **SS-*R*** crystals have tilted columns as well;[2] the adjacent molecules are located in the 0°, 30° and 60° directions from the molecular plane,[21] where the ordinary stack corresponds to the 90° direction. In the present complex, the 30° interaction is maintained as an AA interaction, and the 0° interaction is replaced by a DA interaction.

As an exception, (coronene)(**SO-Et**) has an ordinary 90° stack (Fig. 5(e)), where the mixed stack does not have a short-axis offset and only has a long-axis offset (Fig. 5(f)). The stacking axis is the *a* axis, and the molecular planes are nearly perpendicular to the stacking axis.

Accepted manuscript

Table 2. Crystallographic data of **OS-*R*** and **SO-Et** complexes.

	(pyrene) (**OS-Et**)	(perylene) (**OS-Et**)	(perylene) (**OS-Pr**)	(pyrene) (**SO-Et**)	(perylene) (**SO-Et**)	(coronene) (**SO-Et**)
Formula	$C_{26}H_{20}N_2O_2S_4$	$C_{30}H_{22}N_2O_2S_4$	$C_{32}H_{26}N_2O_2S_4$	$C_{26}H_{20}N_2O_2S_4$	$C_{30}H_{22}N_2O_2S_4$	$C_{34}H_{22}N_2O_2S_4$
Formula weight	570.70	570.76	598.81	520.70	570.76	618.80
Crystal System	triclinic	triclinic	triclinic	triclinic	triclinic	triclinic
Space Group	*P*−1	*P*−1	*P*−1	*P*−1	*P*−1	*P*−1
Shape	plate	plate	plate	plate	plate	plate
a (Å)	7.317(4)	7.326(3)	7.365(3)	7.506(4)	7.699(2)	8.640(8)
b (Å)	7.754(14)	8.145(4)	8.101(8)	7.856(7)	8.464(8)	9.630(5)
c (Å)	11.041(5)	11.233(4)	12.063(4)	10.872(4)	10.046(4)	9.702(5)
α (deg.)	104.81(7)	92.52(3)	88.18(6)	69.79(5)	85.13(5)	107.84(4)
β (deg.)	101.31(4)	103.51(3)	82.11(3)	76.82(4)	83.78(3)	108.51(5)
γ (deg.)	91.40(9)	97.61(4)	83.41(6)	89.71(6)	89.63(4)	101.57(6)
V (Å^3)	592(11)	644.0(5)	708.1(8)	583.8(7)	648.4(7)	687.9(9)
Z-value	1	1	1	1	1	1
T (K)	298	298	298	298	298	298
D_{calc} (g cm^{-3})	1.460	1.472	1.404	1.481	1.462	1.494
Total reflns.	3696	4397	4827	4001	4456	4724
Unique reflns.	3460	3760	4132	3417	3771	4004
(R_{int})	(0.0731)	(0.0735)	(0.1337)	(0.0766)	(0.1267)	(0.1147)
R_1 [$F^2 > 2\sigma(F^2)$]	0.0896	0.0767	0.0896	0.0550	0.0745	0.0755
wR_2 [All reflections]	0.2946	0.2532	0.2326	0.1732	0.2404	0.2391
GOF	1.009	0.967	1.049	1.017	1.004	1.085
DA spacing (Å)	3.45	3.43	3.44	3.54	3.50	3.45

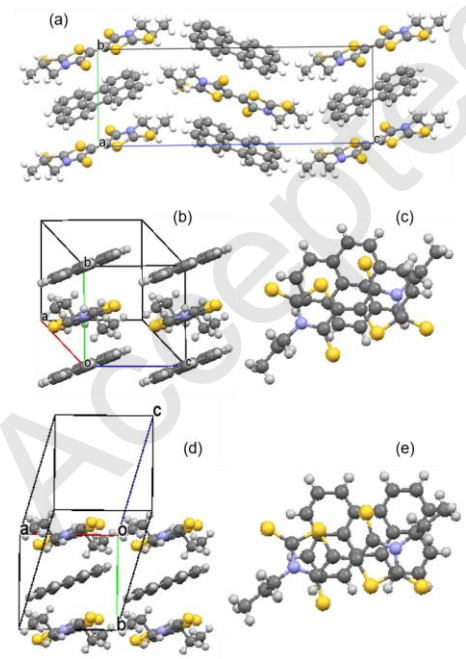


Figure 3. (a) Double-layer structure of (perylene)(**SS-Pr**). (b) Crystal structure of (pyrene)(**SS-Pr**) viewed along the acceptor long axis, and (c) viewed perpendicular to the molecular plane. (d) Crystal structure of (perylene)(**SS-Pr**) viewed along the acceptor long axis, and (e) viewed perpendicular to the molecular plane.

There are large variations in the molecular overlapping mode. When (pyrene)(**SS-Et**) is viewed perpendicular to the molecular plane (Fig. 2(b)), the pyrene molecule is considerably rotated (63°) from the direction of the central C=C bond of the A molecule. The pyrene rotation angles are 11° in **SS-Pr** (Fig. 3(c)), 61° in **OS-Et** (Fig. 4(b)), and 62° in **SO-Et** (Fig. 5(b)). Similar variations of rotation angles are observed in the substituted TCNQ complexes.[15,22] The large molecular rotation is, however, not an adequate condition of the short-axis offset; for example, (pyrene)(TCNQ) makes an ordinary stack in spite of the large rotation.[15,22] In the present complex, offset of the molecular center is the origin of the tilted stack (Fig. 2(b)).

For the perylene complexes, the **SS-Et** molecule of (perylene)(**SS-Et**) is located on the lower half of the perylene molecule (Fig. 2(d)), which is the origin of the short-axis offset. This is reminiscent of (perylene)(TCNQ).[15,23] The overlapping pattern is basically the same in other perylene complexes (Figs. 3(e), 4(d), 4(f), and 5(d)). Perylene molecules are almost parallel to the acceptor C=C direction, but the rotation is not negligible in 15° for **OS-Et** and 9° for **OS-Pr** (Figs. 4(d) and 4(f)).

Accepted manuscript

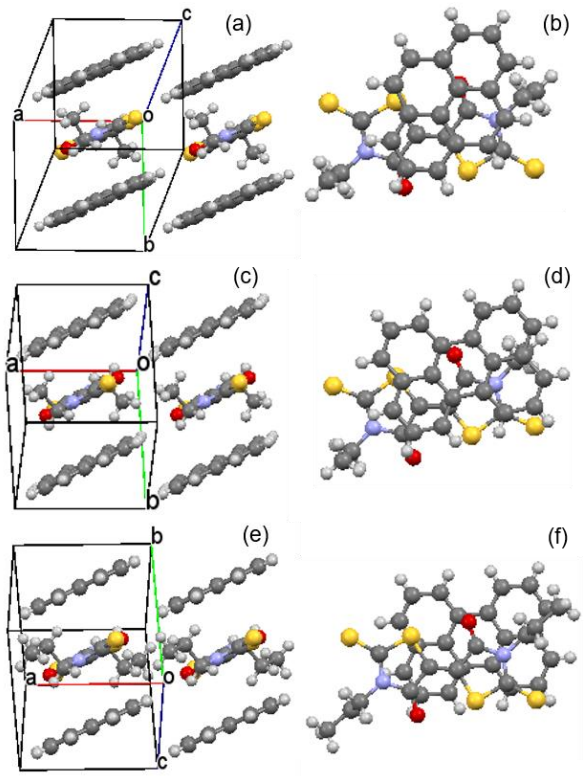


Figure 4. (a) Crystal structure of (pyrene)(**OS-Et**) viewed along the acceptor long axis, and (b) viewed perpendicular to the molecular plane. (c) Crystal structure of (perylene)(**OS-Et**) viewed along the acceptor long axis, and (d) viewed perpendicular to the molecular plane. (e) Crystal structure of (perylene)(**OS-Pr**) viewed along the acceptor long axis, and (f) viewed perpendicular to the molecular plane.

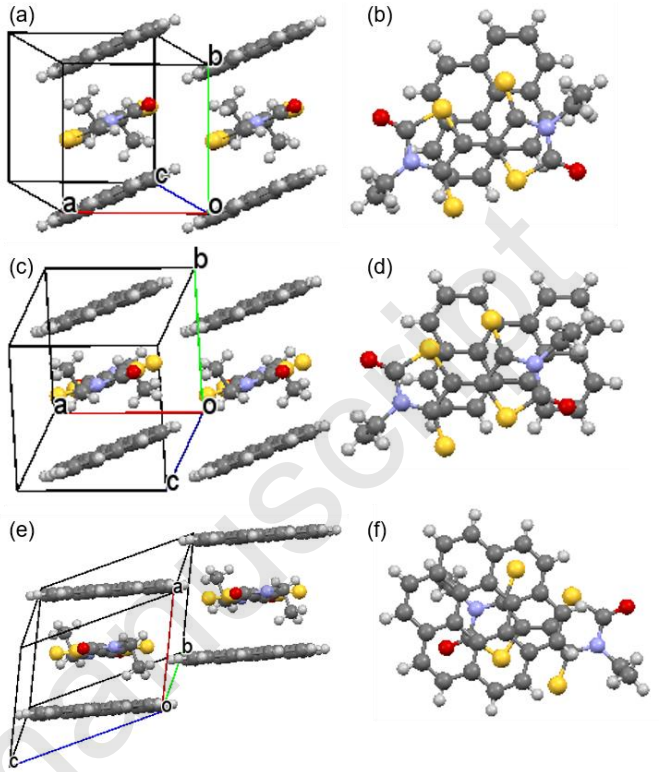


Figure 5. (a) Crystal structure of (pyrene)(**SO-Et**) viewed along the acceptor long axis, and (b) viewed perpendicular to the molecular plane. (c) Crystal structure of (perylene)(**SO-Et**) viewed along the acceptor long axis, and (d) viewed perpendicular to the molecular plane. (e) Crystal structure of (coronene)(**SO-Et**) viewed along the acceptor long axis, and (f) viewed perpendicular to the molecular plane.

In (coronene)(**SS-Et**), the molecules are more tilted (Fig. 2(e)) due to the large coronene molecule as reflected in the small γ angle (Table 1). The **SS-Et** molecule is located above the edge of the coronene molecule (Fig. 2(f)). Displacement from the donor center is less than an aromatic ring (2.8 Å) in perylene, but larger than an aromatic ring in coronene. The largely displaced molecular overlap is similar to (coronene)(TCNQ).[24] The AA 30° interaction seems to be maintained by this large displacement (Fig. 2(e)). The molecular long axis of the acceptor is parallel to the coronene armchair edge in the TCNQ complex, but parallel to the zigzag edge in the present complex (only rotated by 13°). In (coronene)(**SO-Et**), the coronene molecule is rotated by 10° from the direction of the acceptor C=C bond (Fig. 5(f)).

(Pyrene)(**SS-Pr**) and (perylene)(**SS-Pr**) have a double-layer structure along the molecular long axis (Fig. 3(a)); the *c* axis is doubled, and the space group is monoclinic (Table 1). The space group of the pyrene compound ($P2_1/n$) is different from that of the perylene compound ($P2_1/c$) due to the alternate arrangement of the columns. In (perylene)(**OS-Pr**), however, the *c* axis is not doubled.

Comparing bond lengths with those of neutral **SS-Et** and **SS-Et**$^-$ in [Fe(Cp*)$_2$][**SS-Et**],[5a] we can estimate charge-transfer degree ρ in the **SS-Et** complexes (Table S1). The results demonstrate ρ is practically zero. In other cases, bond lengths are also close to the pure acceptors, indicating the basically neutral character of the charge-transfer complexes. This is reasonable in view of the comparatively weak donor ability of the present donors (Fig. 1).

(Perylene)(**SS-Et**) and (coronene)(**SS-Et**) respectively have short S···S contacts of 3.59 and 3.56 Å in the interchain (30°) direction, whereas other **SS-*R*** complexes do not have S···S contacts shorter than 3.9 Å (Table 1). **OS-*R*** and **SO-*R*** complexes do not have any short S···S contacts, although (perylene)(**SO-Et**) has S···S contacts of 3.74 and 3.97 Å. In (coronene)(**SO-Et**), intercolumnar AA interaction disappears entirely. This is associated with the ordinary stacking structure coming from the large coronene molecule.

Accepted manuscript

Table 3. Transistor characteristics of the single-crystal transistors.

Compounds	Conditions	Measurement		μ_{max} [$\mu_{average}$] ($cm^2\ V^{-1}\ s^{-1}$)	V_{th} (V)	on/off ratio
(perylene)(**SS-Et**)	Pristine	under vacuum	e	$0.03\ [4.5 \times 10^{-3}]$	13	4×10^2
		in air		0.05	-2	60
	two months	under vacuum		0.03	13	4×10^2
	under vacuum	in air		0.05	-2	60
(coronene)(**SS-Et**)	Pristine	under vacuum	e	$3.8 \times 10^{-3}\ [1.9 \times 10^{-3}]$	15	1×10^5
		in air		6.5×10^{-3}	2	3×10^6
	two months	under vacuum		4.4×10^{-3}	26	1×10^4
	under vacuum	in air		4.2×10^{-3}	21	7×10^5
(pyrene)(**SS-Pr**)	Pristine	under vacuum	e	2.2×10^{-5}	-20	6
		in air		-	-	-
(pyrene)(**OS-Et**)	Pristine	under vacuum	h	2.1×10^{-3}	-40	1×10^4
			e	4.9×10^{-5}	-17	2×10^4
		in air	h	4.3×10^{-4}	-6	6×10^4
			e	-	-	-
	two months	under vacuum	h	-	-	-
	under vacuum		e	3.9×10^{-4}	30	3×10^4
		in air	h	1.8×10^{-4}	-54	3×10^3
			e	2.1×10^{-4}	10	9×10^4
(perylene)(**OS-Et**)	Pristine	under vacuum	h	$0.012\ [4.9 \times 10^{-3}]$	8	7×10^2
			e	$7.5 \times 10^{-3}\ [1.8 \times 10^{-3}]$	29	3×10^4
		in air	h	$4.1 \times 10^{-3}\ [3.9 \times 10^{-3}]$	1	6×10^4
			e	$1.7 \times 10^{-3}\ [1.2 \times 10^{-3}]$	22	2×10^4
	two months	under vacuum	h	$2.5 \times 10^{-3}\ [9.5 \times 10^{-4}]$	3	1×10^3
	under vacuum		e	$1.5 \times 10^{-3}\ [4.6 \times 10^{-4}]$	40	2×10^4
		in air	h	$7.0 \times 10^{-3}\ [1.9 \times 10^{-3}]$	3	4×10^4
			e	$6.2 \times 10^{-4}\ [3.2 \times 10^{-4}]$	53	3×10^4
(perylene)(**OS-Pr**)	Pristine	under vacuum	h	$7.8 \times 10^{-4}\ [6.8 \times 10^{-4}]$	-27	4×10^5
		in air		8.2×10^{-5}	-23	8×10^3
	two months	under vacuum		3.2×10^{-5}	-32	2×10^3
	under vacuum	in air		5.0×10^{-5}	-28	3×10^3
(pyrene)(**SO-Et**)	Pristine	under vacuum	h	2.6×10^{-4}	-13	8×10^3
		in air		4.8×10^{-4}	-24	1×10^4
	two months	under vacuum		1.2×10^{-4}	-30	7×10^3
	under vacuum	in air		1.7×10^{-4}	-58	2×10^2
(perylene)(**SO-Et**)	Pristine	under vacuum	h	$2.0 \times 10^{-3}\ [7.9 \times 10^{-4}]$	19	6×10^2
			e	$2.4 \times 10^{-4}\ [1.5 \times 10^{-4}]$	60	4×10^3
		in air	h	$1.7 \times 10^{-3}\ [1.4 \times 10^{-3}]$	-3	3×10^2
			e	$1.2 \times 10^{-4}\ [9.2 \times 10^{-5}]$	-20	2×10^3
	two months	under vacuum	h	$6.9 \times 10^{-4}\ [5.3 \times 10^{-4}]$	29	2×10^3
	under vacuum		e	$4.7 \times 10^{-4}\ [4.2 \times 10^{-4}]$	13	9×10^3
		in air	h	$1.1 \times 10^{-3}\ [6.1 \times 10^{-4}]$	2	7×10^4
			e	$5.2 \times 10^{-4}\ [4.8 \times 10^{-4}]$	-5	4×10^3

In summary, these complexes generally have mixed stacks tilted along the molecular short axis. This tilted structure resembles the neutral **SS-*R*** structure. The **OS-*R*** and **SO-*R*** complexes realize the same structure as well, though neutral **OS-*R*** and **SO-*R*** have herringbone structures. Accordingly, the **SS-*R*** crystals maintain short S···S contacts in the 30° direction, whereas similar S···S interactions are absent in the **OS-*R*** and **SO-*R*** complexes.

Transistor characteristics

Characteristics of (perylene)(**SS-Et**) and (coronene)(**SS-Et**) single-crystal transistors are shown in Fig. 6. These complexes exhibit n-channel transistor properties. From these characteristics, the transistor parameters are extracted as listed in Table 3. The perylene compound shows electron mobility of 0.05 $cm^2\ V^{-1}\ s^{-1}$. The transistor characteristics are maintained in air, indicating the excellent air stability. The performance does not drop even after two months. In contrast, (pyrene)(**SS-Pr**) shows much reduced transistor properties.

(Perylene)(**OS-Et**) shows ambipolar transistor properties (Fig. 7). The hole mobility is slightly larger than the electron mobility, and amounts to 0.012 $cm^2\ V^{-1}\ s^{-1}$, which is comparable to the electron mobility of (perylene)(**SS-Et**). The hole dominance is also obvious from the output characteristics;

Accepted manuscript

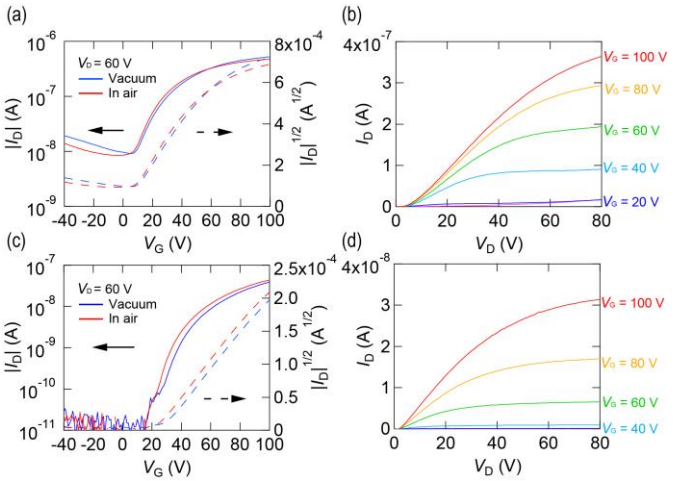


Figure 6. (a) Transfer characteristics of a (perylene)(**SS-Et**) single-crystal transistor measured under vacuum (blue) and in air (red), where the channel length/width are L/W = 113/165 μm. (b) Output characteristics of a (perylene)(**SS-Et**) single-crystal transistor measured under vacuum. (c) Transfer characteristics of a (coronene) (**SS-Et**) single-crystal transistor measured under vacuum (blue) and in air (red), where L/W = 117/112 μm. (d) Output characteristics of a (coronene)(**SS-Et**) single-crystal transistor measured under vacuum.

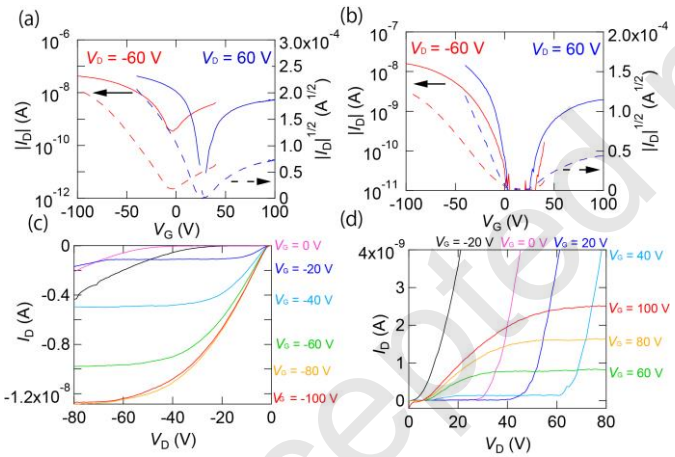


Figure 7. Transfer characteristics of a (perylene)(**OS-Et**) single-crystal transistor measured (a) under vacuum, and (b) in air, where L/W = 165/20 μm. (c,d) Transfer characteristics of a (perylene)(**OS-Et**) single-crystal transistor measured under vacuum.

a remarkable reversed hole-transporting region appears in Fig. 7(d). The difference of the electron and hole threshold voltages V_{th} is around 20 V; the comparatively small value is characteristic of two-component systems.[15,25] However, not only the electron mobility but also the hole mobility drop significantly in air (Fig. 7(b)). The drop of the electron transport is particularly significant. This is the same as **OS-*R***.[2] Therefore, the air-stable n-channel performance of the **SS-Et** compounds is ascribed to **SS-Et**.

(Pyrene)(**OS-Et**) and (perylene)(**SO-Et**) exhibit ambipolar transistor properties as well, while the electron mobility is one order of magnitude smaller than the hole mobility. In (perylene)(**OS-Pr**) and (pyrene)(**SO-Et**), only the hole mobility is estimated. Since even the hole mobilities (< 10^{-3} cm^2 V^{-1} s^{-1}) are smaller than the former two (> 10^{-3} cm^2 V^{-1} s^{-1}), the electron transport is considered to be not large enough to be estimated. Therefore, transistor properties of these **OS-Et** and **SO-Et** complexes are basically regarded as hole-dominant ambipolar transport. In the **OS-Et** compounds, even the hole mobility significantly drops in air, whereas the hole mobility of the **SO-Et** compounds is relatively stable. This is in agreement with the slightly stronger acceptor ability of **SO-Et** (−3.9 eV) than **OS-Et** (−3.8 eV).

Transfer integrals

In order to understand the observed transport properties, transfer integrals are investigated. Interstack AA and DD transfers are evaluated from the splitting of the A LUMO or the D HOMO in the dimers (Table 4). In addition, estimations from the overlap of frozen orbitals are listed.[21]

In (perylene)(**SS-Et**) and (coronene)(**SS-Et**), t_{AA} is significantly large, and t_{DD} is smaller than t_{AA}. These two compounds have S···S contacts shorter than 3.6 Å, whereas the other three **SS-*R*** complexes do not have S···S contacts shorter than 3.9 Å (Table 1). Hence large t_{AA} is obviously related to the S···S contacts. The former two compounds show reasonable transistor properties. Electron transport observed in the **SS-*R*** compounds is closely related to the direct AA interaction.

In the **OS-*R*** and **SO-*R*** compounds, t_{AA} vanishes, but moderate t_{DD} remains. This is consistent with the observed hole-dominant transport. Both t_{AA} and t_{DD} are very small in (coronene)(**SO-Et**), while this compound does not show transistor properties. This comes from the ordinary stacking structure, where each component is comparatively isolated.

In order to investigate the transport in the mixed stacks, we have estimated t_e^{eff} and t_h^{eff} from the triads (Table 4). However, these values (< 10 meV) are significantly smaller than the ordinary mixed stacks (~60 meV).[13] This is not surprising because t_{DA} (< 1 meV) is smaller than the ordinary stacks (~300 meV).[13] LUMO of **SS-*R*** has low-symmetry many-node structures (Fig. 1(a)), and orbital overlap with the donor HOMO is expected to be small. In addition, the overlap modes have generally low symmetry. Not only t_{DA} between the D HOMO and the A LUMO, but also other intrastack transfers are small in general, and the resulting t_e^{eff} and t_h^{eff} are small.

SS-*R* is a characteristic molecule due to the low symmetry and the strong S···S contacts directed to particular orientations. As a result, transport along the mixed stack is not the major pathway, but the direct AA interaction is the most important interaction. Electron transport in the present **SS-*R*** complexes is not so small among mixed-stack complexes (typically at most 0.1 cm^2 V^{-1} s^{-1}). However, when **SS-*R*** is replaced by **OS-*R***, even the charge polarity changes entirely. The observed

Accepted manuscript

Table 4. Calculated transfer integrals (meV).

Complex	t (meV)[a]			t_e^{eff}/t_h^{eff} (meV)	
	AA	DD	DA	Triad	Partition
(pyrene)(**SS-Et**)	44(15)	110(20)	(0.1)	9/7	4/1
(perylene)(**SS-Et**)	195(78)	82(16)	(0.7)	1/13	2/1
(coronene)(**SS-Et**)	216(88)	117(25)	(12.8)	1/5	8/1
(pyrene)(**SS-Pr**)	13(100)	62(27)	(0.6)	2/8	12/8
(perylene)(**SS-Pr**)	5(4)	56(8)	(0.4)	2/19	1/8
(pyrene)(**OS-Et**)	3(0.6)	66(14)	(0.5)	7/8	2/2
(perylene)(**OS-Et**)	4(0.5)	19(0)	(1.2)	7/14	2/2
(perylene)(**OS-Pr**)	1(0.1)	50(7)	(0.7)	6/13	2/2
(pyrene)(**SO-Et**)	44(17)	46(9)	(0.1)	5/17	0/5
(perylene)(**SO-Et**)	27(0.3)	55(2)	(0.7)	12/16	6/13
(coronene)(**SO-Et**)	4(0)	12(1)	(1.8)	7/5	5/2

[a] From the HOMO (DD) or LUMO (AA) splitting of the dimers. Values in the parentheses are from the frozen orbital approximation.

mobility seems to be related to the largest transfers among t_{AA}, t_{DD}, and t_e^{eff} (Fig. S5). Although the interchain interactions mainly mediate the charge transport, the polarity switching appears even in the transistor properties measured in the stacking direction.

Conclusions

Crystal structures of eleven charge-transfer cocrystals containing **SS-*R***, **OS-*R***, and **SO-*R*** are determined. These complexes have mixed stacks with short-axis offset. This is associated with the characteristic S···S contacts between the **SS-*R*** molecules that have the same geometry as the neutral **SS-*R*** crystals. There are a large variety of overlap modes and rotation angles in the stacks. Coronene leads to irregular structures; (coronene)(**SS-Et**) has largely tilted molecules, and (coronene)(**SO-Et**) has ordinary stacks.

Single-crystal transistors of **SS-*R*** complexes show electron transport. This is due to the direct interchain AA interaction mediated by the S···S contacts. When the S···S contacts are lost, the **OS-*R*** and **SO-*R*** compounds exhibit hole-dominant ambipolar transport. Even among the **SS-*R*** complexes, those without short S···S contacts do not have large t_{AA}, and do not show transistor properties. The n-channel transistor properties are air stable in the **SS-*R*** compounds, but not in the **OS-*R*** and **SO-*R*** compounds; the device air stability is similar to the parent acceptors.

It is characteristic of these compounds that the intra-columnar transfers are not most important, but the direct interchain AA interactions are the dominant factor. This should be related to the comparatively low symmetry of the acceptor molecules as well as the characteristic S···S interactions. The observed transistor properties are exceptional among mixed-stack compounds, but the present example demonstrates a case in which only one component is overwhelming in determining the transport properties.

Acknowledgements

This work was partly supported by JSPS KAKENHI Grant Number 18H02044, and Takahashi Industrial and Economic Research Foundation.

Notes and references

[a] *Department of Materials Science and Engineering, Tokyo Institute of Technology, O-okayama 2-12-1, Meguro-ku, 152-8552, Japan. E-mail: mori.t.ae@m.titech.ac.jp*

[b] *Univ Rennes, CNRS, ISCR (Institut des Sciences Chimiques de Rennes) - UMR 6226, F-35000 Rennes, France.*

† Electronic supporting information (ESI) available: CCDC 1932211-1932221 contain the supplementary crystallographic information. Additional information for structure analysis, selected bond lengths, transistor characteristics, and transfer calculations.

1 A. Filatre-Furcate, T. Higashino, D. Lorcy and T. Mori, *J. Mater. Chem. C*, 2015, **3**, 3569.

2 K. Iijima, Y. Le Gal, T. Higashino, D. Lorcy and T. Mori, *J. Mater. Chem. C*, 2017, **5**, 9121.

3 K. Iijima, Y. Le Gal, D. Lorcy and T. Mori, *RSC Adv.*, 2018, **8**, 18400.

4 (a) N. Tenn, N. Bellec, O. Jeannin, L. Piekara-Sady, P. Auban- Senzier, J. Iñiguez, E. Canadell and D. Lorcy *J. Am. Chem. Soc*., 2009, **131**, 16961; (b) Y. Le Gal, T. Roisnel, P. Auban-Senzier, T. Guizouarn and D. Lorcy, *Inorg. Chem*., 2014, **53**, 8755; (c) A. Filatre-Furcate, T. Roisnel, M. Fourmigue, O. Jeannin, N. Bellec, P. Auban-Senzier and D. Lorcy, *Chem. Eur. J*., 2017, **23**, 16004; (c) Y. Le Gal, T. Roisnel, P. Auban-Senzier, N. Bellec, J. Íñiguez, E. Canadell and D. Lorcy, *J. Am. Chem. Soc*., 2018, **140**, 6998.

5 (a) Y. Le Gal, N. Bellec, F. Barrière, R. Clérac, M. Fourmigué, V. Dorcet, T. Roisnel and D. Lorcy, *Dalton Trans*., 2013, **42**, 16672; (b) Y. Le Gal, D. Ameline, N. Bellec, A. Vacher, T. Roisnel, V. Dorcet, O. Jeannin and D. Lorcy, *Org. Biomol. Chem*., 2015, **15**, 8479; (c) Y. Le Gal, M. Rajkumar, A. Vacher, V. Dorcet, T. Roisnel, M. Fourmigué, F. Barrière, T. Guizouarn and D. Lorcy, *CrystEngComm*, 2016, **18**, 3925.

6 (a) K. P. Goetz, D. Vermeulen, M. E. Payne, C. Kloc, L. E. Mcneil and O. D. Jurchescu, *J. Mater. Chem. C*, 2014, **2**, 3065; (b) J. Zhang, W. Xu, P. Sheng, G. Zhao and D. Zhu, *Acc. Chem. Res.*, 2017, **50**, 1654; (c) H. Jiang, P. Hu, K. K. Zhang, Y. Long, W. Hu and C. Kloc, *J. Mater. Chem. C*, 2018, **6**, 1884; (d) T. Mori, *Chem. Lett.*, 2011, **40**, 428.

Accepted manuscript

7 (a) B. Lüssem, M. Riede and K. Leo, *Phys. Status Solidi A*, 2013, **210**, 9; (b) I. Salzmann, G. Heimel, M. Oehzelt, S. Winkler and N. Koch, *Acc. Chem. Res*., 2016, **49**, 370.

8 J. Zhang, J. Jin, H. Xu, Q. Zhang and W. Huang, *J. Mater. Chem. C*, 2018, **6**, 3485.

9 (a) Y. Zhao, Y. Guo and Y. Liu, *Adv. Mater.*, 2013, **25**, 5372; (b) Y. Olivier, D. Niedzialek, V. Lemaur, W. Pisula, K. Müllen, U. Koldemir, J. R. Reynolds, R. Lazzaroni, J. Cornil and D. Beljonne, *Adv. Mater.*, 2014, **26**, 2119; (c) J. Choi, H. Song, N. Kim and F. S. Kim, *Semicond. Sci. Technol.*, 2015, **30**, 64002; (d) L. Lu, T. Zheng, Q. Wu, A. M. Schneider, D. Zhao and L.Yu, *Chem. Rev.*, 2015, **115**, 12666; (e) C. Cheng, H. Geng, Y. Yi and Z. Shuai, *J. Mater. Chem. C*, 2017, **5**, 3247.

10 (a) L. Zhu, Y. Yi, Y. Li, E.-G. Kim, V. Coropceanu and V. J.-L. Brédas, *J. Am. Chem. Soc.*, 2012, **134**, 2340; (b) L. Zhu, Y. Yi, A. Fonari, N. S. Corbin, V. Coropceanu and J.-L. Brédas, *J. Phys. Chem. C*, 2014, **118**, 14150.

11 (a) J. Tsutsumi, S. Matsuoka, S. Inoue, H. Minemawari, T. Yamada and T. Hasegawa, *J. Mater. Chem. C*, 2015, **3**, 1976; (b) Y. Shibata, J. Tsutsumi, S. Matsuoka, K. Matsubara, Y. Yoshida, M. Chikamatsu and T. Hasegawa, *Appl. Phys. Lett.*, 2015, **106**, 143303; (c) T. Higashino, M. Dogishi, T. Kadoya, R. Sato, T. Kawamoto and T. Mori, T. *J. Mater. Chem. C*, 2016, **4**, 5981; (d) R. Sato, M. Dogishi, T. Higashino, T. Kadoya, T. Kawamoto and T. Mori, *J. Phys. Chem. C*, 2017, **121**, 6561.

12 (a) H. Geng, X. Zheng, Z. Shuai, L. Zhu and Y. Yi, *Adv. Mater.*, 2015, **27**, 1443; (b) L. Zhu, H. Geng, Y. Yi and Z. Wei, *Phys. Chem. Chem. Phys.*, 2017, **19**, 4418.

13 (a) R. Sato, T. Kawamoto and T. Mori, *J. Mater. Chem. C*, 2019, **7**, 567; (b) K. Iijima, R. Sanada, D. Yoo, R. Sato, T. Kawamoto and T. Mori, *ACS Applied Mater. Interfaces*, 2018, **30**, 10262.

14 (a) R. Sato, D. Yoo and T. Mori, *CrysEngComm*, **21**, 3218 (2019); (b) R. Sato, D. Yoo, T. Higashino and T. Mori, *Chem. Lett*., 2019, **48**, 264.

15 R. Sanada, D. Yoo, R. Sato, K. Iijima, T. Kawamoto and T. Mori, *J. Phys. Chem. C*, **123**, 12088 (2019).

16 (a) M.-H. Yoon, H. Yan, A. Facchetti and T. J. Marks, *J. Am. Chem. Soc.*, 2005, **127**, 10388; (b) S. Tamura, T. Kadoya, T. Kawamoto and T. Mori, *Appl. Phys. Lett.*, 2013, **102**, 63305.

17 K.-J. Baeg, Y.-Y. Noh, J. Ghim, B. Lim and D.-Y. Kim, *Adv. Funct. Mater.*, 2008, **18**, 3678.

18 Y. Kawasugi, H. M. Yamamoto, M. Hosoda, N. Tajima, T. Fukunaga, K. Tsukagoshi and R. Kato, *Appl. Phys. Lett.*, 2008, **92**, 243508.

19 ADF2017.109; Scientific Computing & Modeling (SCM). Theoretical Chemistry; Vrije Universiteit: Amsterdam, The Netherlands. http://www.scm.com.

20 (a) M. J. S. Dewar, E. G. Zoebisch, E. F. Healy and J. J. P. Stewart, *J. Am. Chem. Soc*., 1985, **107**, 3902.

21 T. Mori, A. Kobayashi, Y. Sasaki, H. Kobayashi, G. Saito and H. Inokuchi, *Bull. Chem. Soc. Jpn.*, 1984, **57**, 627.

22 (a) C. K. Prout, I. J. Tickle and J. D. Wright, *J. Chem. Soc. Perkin 2*, **1973**, 528. (b) Q. Zhang, *CSD Commun.*, 2018, DOI: 10.5517/ ccdc.csd.cc1zybx5, CCDC 1845458.

23 (a) I. J. Tickle and C. K. Prout, *J. Chem. Soc. Perkin 2*, **1973**, 720; (b) D. Vermeulen, L. Y. Zhu, K. P. Goetz, P. Hu, H. Jiang, C. S. Day, O. D. Jurchescu, V. Coropceanu, C. Kloc and L. E. McNeil, *J. Phys. Chem. C*, 2014, **118**, 24688.

24 (a) X. Chi, C. Besnard, V. K. Thorsmolle, V. Y. Butko, A. J. Taylor, T. Siegrist and A. P. Ramirez, *Chem. Mater*., 2004, **16**, 5751; (b) J. Zhang, G. Liu, Y. Zhou, G. Long, P. Gu and Q. Zhang, *ACS Appl. Mater. Interfaces*, 2017, **9**, 1183.

25 O. Pitayatanakul, T. Higashino, M Tanaka, H. Kojima, M. Ashizawa, T. Kawamoto, M. Matsumoto, K. Ishikawa and T. Mori, *J. Mater. Chem. C*, 2014, **2**, 9311.

Accepted manuscript